Depletion Kinetics of Niobium Atoms in the Gas Phase

Roy E. McClean,* Mark L. Campbell, and Erica J. Kölsch

Chemistry Department, United States Naval Academy, Annapolis, Maryland 21402

Received: November 8, 1996; In Final Form: February 24, 1997[⊗]

The gas phase depletion kinetics of Nb(a^6D_J,a^4F_J) in the presence of O_2, SO_2, CO_2, N_2O, and NO are reported. Niobium atoms were produced by the 248 nm photodissociation of Nb(C_5H_5)(CO)$_4$ and detected by laser-induced fluorescence. The ground term of Nb($4d^45s^1$ a^6D_J) reacts at or above the collision rate with all of the aforementioned oxidants. The first excited term, Nb($4d^35s^2$ a^4F_J), is not as reactive with these oxidants. Results are interpreted in terms of long-range attractions and valence interactions. Additionally, we report reaction rate constants for ground state Nb interacting with N_2, CH_4, and SF_6. Nb(a^6D_J) is unreactive toward CH_4. Nb(a^6D_J) + N_2 is pressure dependent at 297 K with $k_0 = (2.6 \pm 0.3) \times 10^{-32}$ cm^6 s^{-1} and $k_\infty = (4.1 \pm 0.5) \times 10^{-13}$ cm^3 s^{-1}. Nb(a^6D_J) + SF_6 is temperature dependent with the rate constants given by $k(T) = (1.2 \pm 0.3) \times 10^{-10} \exp[-(4.8 \pm 0.2)$ kcal mol$^{-1}/RT]$ cm^3 s^{-1}. Depletion of the a^4F_J term by N_2, SF_6, and CH_4 is J-dependent.

Introduction

Current research in gas phase transition metal (TM) atom chemistry is due, in part, to the many low-lying states found in many TM atoms. Some of the low-lying excited states have different electron configurations from those of the respective ground states. It has been shown that the chemical reactivities of TM atoms depend, in general, on the TM's electron configuration.[1−7] In the case of O atom abstraction reactions involving TM atoms and small oxygen-containing molecules, TM atomic states evolving from $d^{n-1}s^1$ (n = number of valence electrons) electron configurations generally react at faster rates than the states evolving from $d^{n-2}s^2$ configurations. Presumably, the faster rates are due to the orbital correlation of the TM atom and the formed TM monoxide. Even where a combination of chemical and physical quenching of excited states takes place, states deriving from $d^{n-2}s^2$ electron configurations might still deplete at a slower rate as a result of the more repulsive nature of the filled s^2 orbital.[4]

The resonance interaction model[8] and the electron transfer mechanism[9] have also been used to describe the depletion kinetics of TM atoms with oxidants. The resonance interaction model predicts activation energies and correlates rate constants and activation energies to the sum of ionization potentials (IP) and s−p promotion energies of metals reacting with N_2O. Research on several TM systems has shown that the resonance model is inadequate in explaining the chemical reactivity of TM atoms (with N_2O) because it does not consider d-electrons.[4,10,11] The electron transfer mechanism is also inadequate. However, the results for some TM atoms reacting with molecules having relatively high electron affinities such as NO_2 and SO_2 are consistent with the electron transfer mechanism.[4,12]

In this paper we report the depletion kinetics of Nb(a^6D_J,a^4F_J) by O_2, SO_2, CO_2, N_2O, and NO in order to determine the effect of Nb's electron configuration on its depletion kinetics. The a^6D_J ground term has a $4d^45s^1$ electron configuration, and the first excited term, a^4F_J, has a $4d^35s^2$ electron configuration. The lowest J state of this excited term lies only 1142.79 cm^{-1} above the ground state and thus is easily accessible.[13] A simplified energy level diagram is shown in Figure 1. In these types of experiments where a TM precursor is photodissociated, there is always the possibility that collisional cascading and/or the unimolecular decay of an energized photofragment into the state of interest might be important. Therefore, in addition to conducting experiments in neat argon buffer, we investigated the Nb + oxidant (OX) reactions in the presence of N_2, SF_6, and CH_4. These gases were used in order to test photochemical and physical effects since these molecules are expected to be more efficient quenchers than Ar. We found that Nb reacted with both N_2 and SF_6. Additionally, we compare our results to other TM + OX systems in attempts to determine factors that drive the chemical reactivity of bare TM atoms. The interaction of Nb with CO_2[14] and CH_4[15,16] has been reported. We are unaware of any other studies of the reactions reported in this paper.

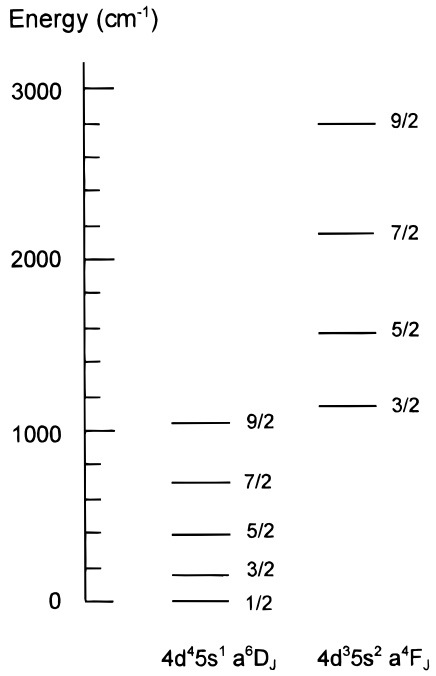

Figure 1. Energy level diagram of atomic niobium for energies less than 3000 cm^{-1}.

Experimental Section

Details of the experimental arrangement have been described in detail elsewhere[17] and are only summarized here. The laser

[⊗] Abstract published in *Advance ACS Abstracts,* April 15, 1997.

S1089-5639(96)03731-0

TABLE 1: LIF Excitation and Detection Information[a]

Nb state[b]	energy (cm^{-1})	λ (nm) of excitation	detection filter (nm)[c]	λ (nm) of detection	detection transition
$a^6D_{1/2}$	0	413.71	400	413.71	$y^6F_{3/2}-a^6D_{1/2}$
				416.37	$y^6F_{3/2}-a^6D_{3/2}$
				420.53	$y^6F_{3/2}-a^6D_{5/2}$
		454.28	600	587.78	$z^4P_{1/2}-a^4P_{1/2}$
				598.32	$z^4P_{1/2}-a^4P_{3/2}$
$a^6D_{3/2}$	154.19	457.48	600	587.78	$z^4P_{1/2}-a^4P_{1/2}$
				598.32	$z^4P_{1/2}-a^4P_{3/2}$
$a^6D_{5/2}$	391.99	442.06	700	684.93	$z^4P_{3/2}-a^4D_{1/2}$
				699.03	$z^4P_{3/2}-a^4D_{3/2}$
				715.94	$z^4P_{3/2}-a^4D_{5/2}$
$a^6D_{7/2}$	695.25	407.97	400	407.97	$y^6F_{9/2}-a^6D_{7/2}$
				413.97	$y^6F_{9/2}-a^6D_{9/2}$
		518.03	520[d]	503.90	$z^6D_{5/2}-a^6D_{3/2}$
				510.02	$z^6D_{5/2}-a^6D_{5/2}$
$a^6D_{9/2}$	1050.26	405.89	400	405.89	$y^6F_{11/2}-a^6D_{9/2}$
$a^4F_{3/2}$	1142.79	403.32	400	385.55	$y^4F_{3/2}-a^6D_{1/2}$
				403.32	$y^4F_{3/2}-a^4F_{3/2}$
				410.68	$y^4F_{3/2}-a^4F_{5/2}$
			600[d]	570.65	$y^4F_{3/2}-a^4D_{1/2}$
				580.40	$y^4F_{3/2}-a^4D_{3/2}$
				592.02	$y^4F_{3/2}-a^4D_{5/2}$
$a^4F_{5/2}$	1586.90	519.31	550	535.07	$z^4D_{5/2}-a^4F_{7/2}$
$a^4F_{7/2}$	2154.11	516.44	550	534.42	$z^4D_{7/2}-a^4F_{9/2}$
$a^4F_{9/2}$	2805.36	403.25	400	384.36	$y^4D_{7/2}-a^4F_{5/2}$
				392.93	$y^4D_{7/2}-a^4F_{7/2}$
				403.25	$y^4D_{7/2}-a^4F_{9/2}$

[a] References 13 and 18. [b] The ground and excited terms evolve from $4d^45s^1$ and $4d^35s^2$ orbital occupancies, respectively. [c] Broad-band filter with fwhm = 50 nm, except for the 520 nm filter which has fwhm = 10 nm. [d] Filter is angled to give the maximum percent transmission of the LIF signal.

photolysis/laser-induced fluorescence (LP/LIF) technique was used in this work. The reaction chamber was a stainless steel cross with gas inlet and outlet ports, a viewport for LIF detection, and windows for passage of the laser beams; the chamber was contained in a convection oven capable of attaining temperatures up to 623 K. The niobium precursor, $Nb(C_5H_5)(CO)_4$, was entrained in a flow of argon gas and carried to the reaction chamber. A slow flow of argon passed over the windows in order to minimize the deposition of the precursor and photofragments. The buffer (Ar or Ar/CH_4), window, and reactant gases passed through mass flow controllers prior to admission to the reaction chamber. The carrier gas passed through a mass flow meter prior to entraining the precursor. Total flows were between 150 and 6000 sccm, depending on total pressure. Partial pressures of the individual components were determined by their relative flows and the total pressure in the reaction chamber. Pressures were measured by Baratron manometers and temperatures were measured with a thermocouple attached to the reaction chamber.

Niobium atoms were produced from $Nb(C_5H_5)(CO)_4$ by either the focused or unfocused output of an excimer laser operating on KrF (248 nm) at 15 or 21 Hz. Rate constant measurements did not depend on the photolysis fluences which were between 0.1 and 1. J cm^{-2} in the reaction chamber. Detection of Nb atoms was by LIF using laser light from an excimer-pumped dye module. The photolysis and dye beams counterpropagated through the chamber. Neutral density filters were used to ensure that the dye laser fluence did not affect the kinetic results. Dye laser fluences were less than 1 mJ/pulse. The Nb states studied and the corresponding excitation wavelengths and interference filters used are listed in Table 1. A photomultiplier tube and lens focusing system, situated 90° to the laser beams, collected the LIF signal which was subsequently sent to a gated boxcar sampling module, and the boxcar's output was stored and analyzed by a computer.

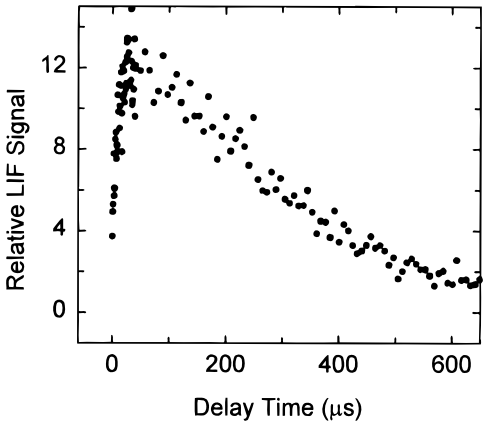

Figure 2. Production and decay of $Nb(a^6D_{1/2})$ following the 248 nm photodissociation of $Nb(C_5H_5)(CO)_4$ in Ar buffer. T = 298 K, P_{tot} = 20 Torr, photolysis laser fluence ≈ 100 mJ cm^{-2}.

All kinetic results are based on the disappearance of Nb atoms under pseudo-first-order conditions where the number density of Nb, [Nb], was much less than the number density of the other reactants. Reaction time was taken as the delay time between the laser pulses. For a given experimental run, the delay time was varied by a digital delay generator controlled by a computer. Minimum delay times were typically 1−3 μs in order to prevent overlap of the prompt emission with the LIF signal. The trigger source for these experiments was scattered pump laser light incident upon a fast photodiode. LIF decay traces consisted of 200−500 points, each point averaged over 2−10 laser shots. LIF intensities were proportional to Nb number densities.

Reagents. The following reagents were used as received: $Nb(C_5H_5)(CO)_4$,[19] Ar (Potomac Airgas, Inc., 99.998%), N_2 (Potomac Airgas, Inc., 99.998%), SF_6 (Air Products, 99.9%; Rockwell International, Corp., >99.9%), CH_4 (Linde, ultrahigh purity grade), O_2 (MG Industries, 99.8%), SO_2 (MG Industries, 99.98%), CO_2 (MG Industries, anaerobic grade, 99.9%), N_2O (Union Carbide, 99.0%), and NO (Liquid Carbonic, 99.0%).

Data Analysis and Results

Experiments were typically carried out at 20 Torr total pressure and room temperature. Selected Nb + reactant systems were studied as a function of temperature and/or total pressure. Partial pressures of $Nb(C_5H_5)(CO)_4$ are not known. However, on the basis of the carrier flow rate, total flow rate, and total pressure, we estimate the partial pressure of $Nb(C_5H_5)(CO)_4$ in the reaction chamber to be very much less than 0.1 mTorr for all experiments.

Significant growth of ground state $Nb(a^6D_{1/2})$ following the photodissociation of $Nb(C_5H_5)(CO)_4$ in argon buffer was observed, as shown in Figure 2. This growth is attributed mainly to the collisional quenching from higher Nb states and, possibly, to dissociation of long-lived photofragments. Addition of oxidant appeared to significantly reduce (or eliminate) the growth. To ensure the growth was not affecting the reaction rates, the oxidation reactions were studied in the presence of other relatively inert gases that are expected to be better quenchers than Ar. N_2 and SF_6 were considered as buffers but were slightly reactive with ground state Nb. CH_4 was found to be the buffer of choice. We conducted experiments at 20 Torr total pressure with approximately 5, 9, 15, and 19 Torr of CH_4 (balance Ar). For a given $Nb(a^6D_J)$ + OX system, identical rate constants were measured for methane partial pressures of 9 Torr or greater. The rate constants for 0−5 Torr of CH_4 were systematically lower than the measured rate constants in higher partial pressures of CH_4. Thus, in the absence of sufficient

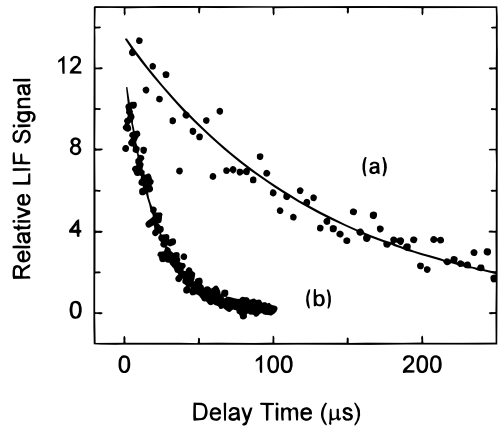

Figure 3. Temporal behavior of Nb($a^6D_{1/2}$) in the absence and presence of O_2 in CH_4/Ar buffer. $T = 298$ K, $P_{tot} = 20$ Torr. Solid lines through the data are exponential fits. (a) $P_{CH_4} = 9.9$ Torr, $\tau = 131$ μs. (b) $P_{CH_4} = 9.9$ Torr, $P_{O_2} = 4.51$ mTorr, $\tau = 21.6$ μs.

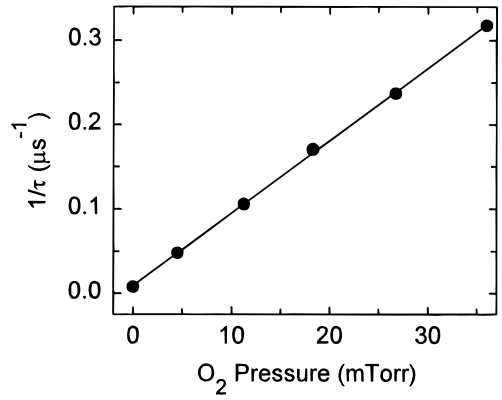

Figure 4. Typical plot for determining second-order rate constants. Conditions are the same as in Figure 3b except for the changing O_2 pressure. The slope yields $k = (2.64 \pm 0.03) \times 10^{-10}$ cm^3 s^{-1}, where the uncertainty represents one standard deviation in the regression fit.

methane, growth processes were still significant, and the growth affected the rate constant measurements even though the growth appeared to have been eliminated with the addition of oxidants. There was no indication of reaction between Nb($a^6D_{1/2}$) and CH_4. This result is consistent with other studies of Nb reacting with CH_4 and other straight-chain alkanes.[15,16]

Figure 3 shows an exponential decay plot of Nb($a^6D_{1/2}$) in the presence of CH_4 and O_2. Note that the growth in the $a^6D_{1/2}$ state in the absence of O_2 (Figure 3a) is dramatically reduced due to the efficient quenching of the excited states of Nb by CH_4. The solid line through the data is an exponential fit to the equation

$$I = I_0 \exp(-t/\tau) \quad (1)$$

where I and I_0 are the LIF signals at time t and time $t = 0$, respectively, and τ is the lifetime from which the pseudo-first-order rate constant, $1/\tau$, is obtained. $1/\tau$ is given by

$$1/\tau = 1/\tau_0 + k[\mathrm{RCT}] \quad (2)$$

where τ_0 is the lifetime of Nb without added reactant, RCT, and k is the second-order rate constant. τ_0 represents the lifetime of Nb in the presence of other species in the reaction chamber and diffusion out of the detection zone. τ_0 was usually long compared to τ with added reactant. Second-order rate constants were obtained from the slopes of plots of $1/\tau$ vs reactant partial pressure such as that shown in Figure 4. The overall uncertainties of the measured second-order rate constants are estimated at $\pm$30% and take into consideration the reproducibility of k and instrumental uncertainties such as digital delay and flow measurements.

TABLE 2: Measured Second-Order Rate Constants for the Depletion of Nb($a^6D_{1/2}$,a^4F_J) by N_2[a]

Nb state	P (Torr)	k (cm^3 s^{-1})	Nb state	P (Torr)	k (cm^3 s^{-1})
$a^6D_{1/2}$	10	1.8×10^{-14}	$a^4F_{3/2}$	20	4.7×10^{-13} [b]
	20	2.9×10^{-14}	$a^4F_{5/2}$	20	3.9×10^{-13}
	50	4.5×10^{-14}	$a^4F_{7/2}$	20	3×10^{-13} [c]
	100	7.1×10^{-14}	$a^4F_{9/2}$	20	5.3×10^{-14}
	150	1.0×10^{-13}			
	200	1.1×10^{-13}			
	250	1.4×10^{-13}			
	300	1.6×10^{-13}			
	400	1.8×10^{-13}			
	500	2.2×10^{-13}			
	600	2.3×10^{-13}			
	20	1.1×10^{-14} (450 K)			

[a] Buffer = Ar and $T = 296$ K, except where noted. Uncertainties are $\pm$30% except where noted. At 20 and 100 Torr total pressure, the $a^6D_{9/2}$ state has measured rate constants identical (within experimental uncertainty) to those of the ground state. [b] Determined from biexponential fits to decay data; uncertainty = $\pm$50%; $k_2 \approx 5 \times 10^{-14}$ cm^3 s^{-1}. [c] Order of magnitude estimate; underlying structure present.

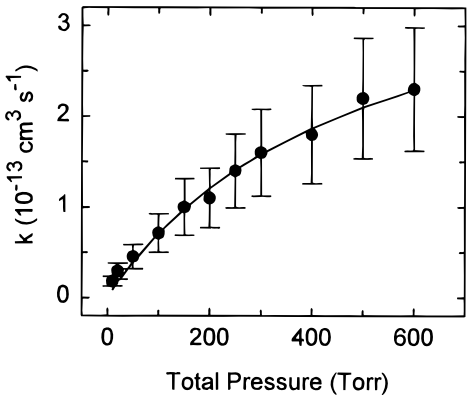

Figure 5. Second-order rate constants of Nb($a^6D_{1/2}$) + N_2 as a function of total pressure. $T = 296$ K, buffer = Ar. Error bars represent $\pm$30% uncertainties. Solid line is a fit to eq 3. See text for results of fit.

LIF lines indicative of a molecular substance were observed following excitation at approximately 516 nm using a 550 nm broad-band filter (fwhm = 50 nm). As seen in Table 1, Nb($a^4F_{7/2}$) was excited at 516.44 nm. The molecular structure was negligibly small in the presence of added O_2, CO_2, and NO. In the presence of added SO_2 and N_2O, the LIF from Nb($a^4F_{7/2}$) was very intense compared to the weak molecular signal at relatively short decay times; however, the long time temporal behavior was affected by the underlying molecular structure. Only an estimate of the rate constant is reported in these (few) cases.

Nb + N_2. The decay kinetics of Nb + N_2 were studied in argon buffer. The short time growth exhibited in the decay of Nb($a^6D_{1/2}$) in argon buffer was unimportant because the observed lifetimes in the presence of N_2 were relatively long. Data were collected at room temperature as a function of total pressure. Measured rate constants are listed in Table 2 and are shown graphically in Figure 5. The solid line through the data is a weighted fit to the simplified Lindemann−Hinselwood expression[20]

$$k = k_0[\mathrm{M}]/(1 + k_0[\mathrm{M}]/k_\infty) \quad (3)$$

where k_0 is the limiting low-pressure third-order rate constant, k_∞ is the limiting high-pressure second-order rate constant, and [M] is the buffer gas number density. Results of the fit are

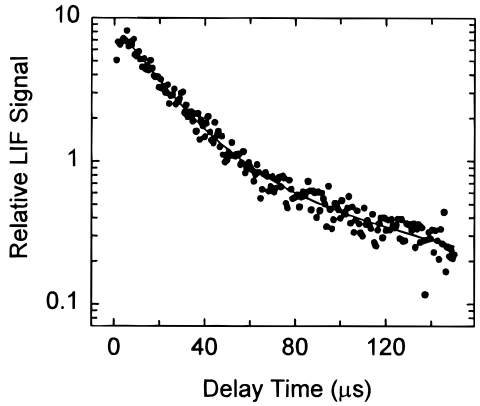

Figure 6. Biexponential behavior of Nb($a^4F_{3/2}$) in the presence of N_2. $T = 298$ K, $P_{tot} = 20$ Torr, $P_{N_2} = 2.65$ Torr, buffer = Ar. Solid line is a biexponential fit with $\tau_1 = 19.0$ μs and $\tau_2 = 108$ μs.

$$k_0 = (2.6 \pm 0.3) \times 10^{-32}\ \text{cm}^6\ \text{s}^{-1},$$
$$k_\infty = (4.1 \pm 0.5) \times 10^{-13}\ \text{cm}^3\ \text{s}^{-1}$$

where the uncertainties indicate one standard deviation. The rate constant of Nb($a^6D_{1/2}$) + N_2 at 450 K and 20 Torr total pressure is smaller than that at 298 K and 10 Torr total pressure, as shown in Table 2. At 20 and 100 Torr total pressure, the $a^6D_{9/2}$ state has depletion rate constants that are identical, to within experimental uncertainty, to those of the ground state.

The measured rate constants for Nb(a^4F_J) + N_2 are also listed in Table 2. The $a^4F_{3/2}$ state exhibited biexponential temporal behavior as shown in Figure 6. The temporal behavior of Nb($a^4F_{3/2}$) appears exponential for an approximately 10-fold number density range after which a slower decay is observed. The solid line through the data is a fit to the biexponential expression

$$I = A_1 \exp(-t/\tau_1) + A_2 \exp(-t/\tau_2) \qquad (4)$$

where A_1 and A_2 are constants and τ_1 and τ_2 are the short and long lifetimes, respectively. Both τ_1 and τ_2 depended on the pressure of N_2. Second-order rate constants from τ_1 and τ_2 are obtained from plots such as that shown in Figure 4. We estimate the overall uncertainty of the second-order rate constant from τ_1 at ± 50%. Due to the relatively small magnitude of the long time temporal behavior shown in Figure 6 (and all other data exhibiting biexponential behavior), uncertainties of the second-order rate constant, k_2, obtained from τ_2, are relatively large. For the Nb($a^4F_{3/2}$) + N_2 system, we attribute τ_1 to the chemical and/or physical quenching of Nb($a^4F_{3/2}$). τ_2 might represent the slower decay of the $a^4F_{9/2}$ state since $k(a^4F_{9/2}) \approx k_2(a^4F_{3/2})$. If τ_1 represents the rate of approach of Nb($a^4F_{3/2}$) to a Boltzmann population and the $a^6D_{9/2}$ and $a^4F_{3/2}$ states' intermultiplet mixing rate is fast (the energy separation is only 92.53 cm^{-1}), then τ_2 could alternately represent the depletion rate of Nb($a^6D_{9/2}$). In this case, the $a^4F_{3/2}$ state will be removed at the same rate as the $a^6D_{9/2}$ state if the mixing rate constant is fast relative to the removal rates of the two states. The decay of the $a^4F_{5/2}$ and $a^4F_{9/2}$ states was exponential. The rate constant of Nb($a^4F_{7/2}$) is an estimate because of the underlying molecular structure.

Nb + SF_6 and CH_4. The reaction of Nb($a^6D_{1/2}$) with SF_6 was investigated at room temperature over the total pressure range 10−50 Torr using Ar buffer and as a function of temperature at 20 Torr total pressure. The rate constants were found to be independent of total pressure. Results are tabulated in Table 3 and are shown in Arrhenius form in Figure 7. The Arrhenius equation obtained from the weighted fit in Figure 7 is

TABLE 3: Measured Second-Order Rate Constants for the Depletion of Nb($a^6D_{1/2}$, a^4F_J) by SF_6 and CH_4[a]

SF_6			CH_4		
Nb state	T (K)	k ($cm^3\ s^{-1}$)	Nb state	T (K)	k ($cm^3\ s^{-1}$)
$a^6D_{1/2}$	297	4.6×10^{-14}	$a^6D_{1/2}$	297	NR
	373	1.8×10^{-13}			
	423	3.6×10^{-13}			
	473	7.1×10^{-13}		473	NR
	531	1.3×10^{-12}			
$a^4F_{3/2}$	296	1.1×10^{-12}	$a^4F_{3/2}$	296	2.0×10^{-12}
$a^4F_{5/2}$	296	3.7×10^{-12}	$a^4F_{5/2}$	296	2.8×10^{-12}
$a^4F_{7/2}$	296	4.3×10^{-12}	$a^4F_{7/2}$	296	3.6×10^{-12}
$a^4F_{9/2}$	296	3.2×10^{-11}	$a^4F_{9/2}$	296	7.9×10^{-12}

[a] Buffer = Ar and total pressure = 20 Torr, except where noted. NR = no observed reaction ($k < 10^{-14}$ $cm^3\ s^{-1}$). Uncertainties are ±30%.

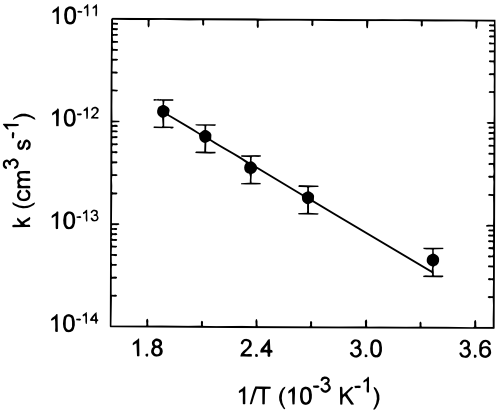

Figure 7. Temperature dependence of Nb($a^6D_{1/2}$) + SF_6. $P_{tot} = 20$ Torr, buffer = Ar. Solid line is a weighted fit to the expression $k(T) = A \exp(-E_a/RT)$. Error bars represent ±30% uncertainties. See text for results of fit.

$$k = (1.2 \pm 0.3) \times 10^{-10} \times$$
$$\exp[-(4.8 \pm 0.2)\ \text{kcal mol}^{-1}/RT]\quad \text{cm}^3\ \text{s}^{-1} \quad (5)$$

where the uncertainties represent one standard deviation. We observed no reaction for Nb($a^6D_{1/2}$) + CH_4 at a total pressure of 20 Torr using argon buffer at 297 and 473 K. Depletion of the a^4F_J term by SF_6 and CH_4 was investigated at room temperature and 20 Torr total pressure using Ar buffer. Results are also listed in Table 3. Note that the rate constants here are larger than the rate constants for Nb(a^4F_J) + N_2. Based on the rate constants in Table 3, for methane pressures of 9 Torr and above, the a^4F_J states are essentially all relaxed within a few microseconds. Thus, relaxation of these states was unimportant when observing the a^6D_J term under these conditions.

Nb + OX. Results for the depletion of Nb by OX are given in Table 4. Most of the rate constants were measured at room temperature and at a total pressure of 20 Torr. The buffer was a mixture of argon and methane for reactions involving the a^6D_J term and only argon for the a^4F_J term. The measured rate constants of all spin−orbit states of the a^6D_J term for a given oxidant are identical, to within experimental uncertainty, and only the averaged value is reported. The rate constants of Nb(a^6D_J) + OX are all on the order of the gas collision rate, with k(Nb + SO_2) being larger than the others. The rate constants of the a^4F_J term are J-dependent, as shown in the table. The depletion of Nb($a^4F_{9/2}$) in the presence of the oxidants was also investigated in N_2 buffer since N_2 is expected to quench highly excited states more efficiently than Ar. Measured rate constants were identical, to within experimental uncertainty, to those obtained in argon buffer. Thus, underlying growth processes

TABLE 4: Measured Second-Order Rate Constants for the Depletion of Nb(a^6D_J,a^4F_J) by Oxidants[a]

		k (10^{-11} cm^3 s^{-1})				
Nb state	T (K)[b]	O_2	SO_2	CO_2	N_2O	NO
a^6D_J	296	25	56	12	24	29
$a^4F_{3/2}$	296	0.98	23	3.0[e]	5.0[f]	3.0
$a^4F_{5/2}$	296	0.71	19	1.4	2.1	2.8
$a^4F_{7/2}$	296	0.53	10[d]	0.96	1[c]	2.3
$a^4F_{9/2}$[c]	296	0.40	15	1.6	1.6	2.4
	373	0.73		1.6	1.7	3.2
	473	1.3		1.6		4.9

[a] Buffer = a combination of CH_4 and Ar for Nb(a^6D_J). Buffer = Ar for the a^4F_J term, except as noted below. Total pressure = 20 Torr, except where noted. Uncertainties = ±30% except where noted. [b] Room temperature = 296 ± 1 K; on some days the temperature was either a little less or a little greater than 296 K. [c] Rate constants of Nb($a^4F_{9/2}$) + OX at 296 K were also measured in N_2 buffer; they are identical, to within experimental uncertainty, to those listed for Ar buffer. [d] Order of magnitude estimate because of underlying structure. [e] Small tail present at relatively long decay times. [f] Obtained from biexponential fits; uncertainty = ±50%; $k_2 \approx 1 \times 10^{-11}$ cm^3 s^{-1}.

from higher lying states were not important in contrast to what was observed for the ground term. The depletion of the a^6D_J and a^4F_J term by N_2 was slow compared to the depletion by the oxidants so that the presence of N_2 at 20 Torr total presence did not affect the depletion kinetics of Nb + OX. From the limited amount of temperature data available, we obtain an A factor and an activation energy for Nb($a^4F_{9/2}$) + O_2 of 9.1×10^{-11} cm^3 s^{-1} and 1.9 kcal mol^{-1}, respectively, and for Nb($a^4F_{9/2}$) + NO we obtain 1.5×10^{-10} cm^3 s^{-1} and 1.1 kcal mol^{-1}. Note that, for a particular Nb + OX system, the rate constants of Nb(a^4F_J) are less than those of the a^6D_J term.

Discussion

Nb + N_2, SF_6, and CH_4. Although NbN has been observed in matrices,[21] our results indicate only a termolecular channel for the reaction of Nb($a^6D_{1/2}$) with N_2. The formation of NbN is not expected to be important under the conditions of our experiment. The smaller second-order rate constant at 450 K and 20 Torr total pressure compared to the room temperature measurement at 10 Torr suggests no significant energy barrier to complex formation. (The effective total number density at 450 K and 20 Torr is greater than that at 296 K and 10 Torr.) However, the relatively small value of the limiting high-pressure second-order rate constant, $k_\infty = 4.1 \times 10^{-13}$ cm^3 s^{-1}, indicates the presence of other rate limiting factors for complex formation. In depletion studies of Nb clusters with N_2, Nb clusters showed a strong size dependency for sizes greater than or equal to three Nb atoms.[22,23] It was emphasized in one of the studies that conclusions on the reactivity of the Nb atom and dimer could not be reached because the lifetime of the formed adducts might be too short to survive in their apparatus.[22] Our study shows that atomic niobium does, in fact, interact with N_2. The extent of reaction of the atom compared to the smaller Nb clusters cannot be made because only relative rates were reported in the other studies. Matrix and theoretical studies on other TM + N_2 systems indicate predominant end-on $C_{\infty v}$ (TM−N−N) and side-on C_{2v} bonded products.[24−29] Where insertion products are indicated, substantial activation barriers are expected.[24] An insertion product for Nb + N_2 seems unlikely in view of the negligible activation barrier in the third-order kinetic regime. (Theoretical studies on the Nb + N_2 system would be most helpful here.) The relatively small value of $k_0 = 2.6 \times 10^{-32}$ cm^6 s^{-1} for Nb + N_2 compared to k_0 of TM + the oxygen-containing molecules NO and O_2 indicates that NbN_2 is not as strongly bound as CrNO, MoNO, CrO_2, NiO_2, and CuO_2.[2]

The results of Nb($a^6D_{1/2}$) + SF_6 are consistent with a bimolecular reaction. The assumed products are NbF and SF_5,

$$\mathrm{Nb} + \mathrm{SF_6} \rightarrow \mathrm{NbF} + \mathrm{SF_5} \qquad (6)$$

Although the bond energy of NbF is not well-known, reaction 6 is expected to be exothermic by approximately 38 kcal mol^{-1}.[30] The electron transfer mechanism (ETM) has been indicated for some reactions involving TM atoms and relatively high electron affinity molecules such as SO_2 (EA = 1.107 eV).[4,30] SF_6 has an electron affinity of 1.05 eV.[30] The calculated 298 K rate constant for Nb + SF_6, based on the electron transfer mechanism[9,31] is 6.9×10^{-11} cm^3 s^{-1}, which is significantly greater than the observed rate constant of 4.6×10^{-14} cm^3 s^{-1}. Thus, the electron transfer mechanism is not operative in the Nb + SF_6 system. Our study of Nb + SF_6 is the first reported rate constant for the reaction of a TM atom with SF_6. The only other study of a TM atom interacting with SF_6 is the chemiluminescence study of Mn + SF_6.[32] Herbertson and Levy have indicated that the best chance for Mn to penetrate to short internuclear distances of SF_6 is through a C_{3v} collision geometry where repulsive potentials are encountered. Such repulsions will likely show as activation energies in temperature-dependent rate investigations such as measured for Nb + SF_6. Rate constant measurements have been reported for Na,[33,34] K,[35] Cs,[36] Ga,[37] Sn,[38] Pb,[39] and Si[40] with SF_6. For those reactions that have been studied as a function of temperature (Na, K, Pb), the Arrhenius preexponential factors are all on the order of 6×10^{-10} cm^3 s^{-1}, and the activation energies range from 2.46 to 7 kcal mol^{-1}. The alkali fluoride electronic states are expected to have some ionic character; thus, the dynamics of Na and K + SF_6 reactions might involve the crossing of ionic and covalent surfaces with correspondingly small energy barriers, as observed. SF_6 + Na and K have measured activation energies of 2.46 and 2.94 kcal mol^{-1}, respectively. Alkali metals have relatively small IPs such that the curve crossings are on the order of the collision distance. k(ETM) for Nb + SF_6 corresponds to a curve crossing of 2.52 Å, which is less than the hard-sphere collision diameter.[41] Thus, an energy barrier is encountered.

Depletion of the a^4F_J term by N_2, SF_6, and CH_4 is J-dependent. We cannot distinguish between physical and chemical quenching. However, since significant growth was indicated in the ground term, we conclude that physical quenching is the major depletion channel. The larger quenching rate constants of SF_6 and CH_4, compared to that of N_2 are consistent with the observation of SF_6 and CH_4 being better energy stabilizers.

Nb + OX. Results of the Nb + OX systems are quite interesting. The ground term, which has a $4d^45s^1$ electron configuration, is very reactive with all of the oxidants investigated. Bimolecular reactions are indicated. The production of NbO on a fully ground state surface is thermodynamically feasible in all cases, with relatively large exothermicities of 68.1, 55.6, 60.1, 147, and 36.3 kcal mol^{-1} for reactions of Nb with O_2, SO_2, CO_2, N_2O, and NO, respectively.[42] The only other thermochemically feasible product is NbC from the concerted reaction of Nb + CO_2, which is approximately thermoneutral.[30] This reaction is considered unlikely in view of the absence of a significant activation energy. There was also no evidence of NbC in a study of Nb_x ($x = 1-13$) + CO_2 by Song et al.[14] An intense NbO mass peak (actually an NbO^+ peak in their detection apparatus) following reaction was observed, however, suggesting an O atom abstraction for atomic niobium. It is worth mentioning that Song et al. also noted that the peak might have resulted from the ionization of another product followed by evaporation of NbO (or NbO^+). Nevertheless, the large rate

TABLE 5: Room Temperature Rate Constants of Selected TM Atom + OX Bimolecular Reactions[a,b]

		k (cm^3 s^{-1})									
TM	config	O_2	ref	SO_2	ref	CO_2	ref	N_2O	ref	NO	ref
Sc	$3d^14s^2$	5.9×10^{-12}	44	*c*		*c*		1.2×10^{-12}	44	9.2×10^{-12}	44
Ti	$3d^24s^2$	1.6×10^{-12}	12, 44, 45	6.1×10^{-11}	12	1.6×10^{-13}	12	5.9×10^{-13}	12, 44, 45	7.4×10^{-12}	12, 44, 45
V	$3d^34s^2$	3.3×10^{-12}	3, 44	*c*		3.3×10^{-13}	3	4.5×10^{-13}	44	1.1×10^{-11}	3, 44
Cr	$3d^54s^1$	*f*	2, 46	*c*		*c*		1.0×10^{-14}	47, 48	*f*	47
Mn	$3d^54s^2$	*f*	2	*c*		*c*		2.9×10^{-18} [e]	10	*c*	
Fe	$3d^64s^2$	*f*	2, 49	*c*		*c*		2.4×10^{-18} [e]	11, 50	*f*	50
Cu	$3d^{10}4s^1$	*f*	2	*c*		*c*		5.7×10^{-18} [e]	51	*c*	
Zn	$3d^{10}4s^2$	*c*		*c*		*c*		1.8×10^{-15} [e]	52	*c*	
Nb[d]	$4d^45s^1$	2.5×10^{-10}		5.6×10^{-10}		1.2×10^{-10}		2.4×10^{-10}		2.9×10^{-10}	
Mo	$4d^55s^1$	1.0×10^{-10}	53, 54	1.3×10^{-10}	4	NR	4, 53	1.3×10^{-17} [e]	4, 53	*f*	4
Ru	$4d^75s^1$	*f*	55	*c*		*c*		1.6×10^{-14}	55	*f*	56
Rh	$4d^85s^1$	*f*	57	*c*		*c*		7.3×10^{-13}	57	*c*	
Ta	$5d^36s^2$	7.3×10^{-12}	58	6.5×10^{-11}	59	2.2×10^{-15}	58	2.9×10^{-13}	58	5.6×10^{-11}	58
W	$5d^46s^2$	1.6×10^{-12}	17	6.0×10^{-12}	60	NR	60	3.0×10^{-15}	60	2.8×10^{-11}	60
Os	$5d^66s^2$	7.1×10^{-13}	61	*c*		*c*		1.2×10^{-17} [e]	61	*c*	

[a] NR stands for no reaction ($<10^{-15}$ cm^3 s^{-1}). [b] Reference 43. [c] Not measured. [d] This work. [e] Value obtained by extrapolation to 298 K. [f] Termolecular reaction.

constant, the relatively large exothermicity, and no evidence of NbC (or other bimolecular products) in the reaction of Nb with CO_2 strongly suggests the production of NbO.

Although the first excited term, Nb($4d^35s^2$ a^4F_J), with its closed s subshell, is not as reactive as the ground term toward the oxidants, the depletion rate constants of the individual J states are appreciably large. Assuming an Arrhenius preexponential factor of 3×10^{-10} cm^3 s^{-1}, activation energies are only 1−2 kcal mol^{-1}. Note that the $a^4F_{3/2}$ spin−orbit state has the largest rate constant in the term for all oxidants. This state lies only 95.53 cm^{-1} above the highest J state of the ground term. Thus, some mixing between these two adjacent states very likely occurs.

Table 5 compares bimolecular rate constants of ground state TM + OX reactions at 298 K. TMs from all three TM series are represented. (Arrhenius parameters are not available for all of the reactions; however, reactions with rate constants less than 10^{-10} cm^3 s^{-1} are expected to have activation energies, with smaller rate constants corresponding to larger activation energies.) The fast rates observed for Nb + OX are unlike other TM + OX systems that have been reported even though some of the other TM atoms have as their ground states $d^{n-1}s^1$ electron configurations. As seen in the table, Nb is more reactive than all of the other TM atoms. In most cases for a given oxidant, TM atoms with $d^{n-1}s^1$ ground state electron configurations are more reactive than those with $d^{n-2}s^2$ ground state electron configurations. This result is expected based on the repulsive nature of the $d^{n-2}s^2$ configuration and on the orbital correlation of $d^{n-1}s^1$ TM atoms and low-energy states of the TM monoxides.[62] Consider the TM + O_2, SO_2, and NO rate constants. Rate constants of the $d^{n-1}s^1$ TM atoms are clearly larger than the others. The rate constant for Nb + SO_2 is even larger than the calculated collision rate of 2.3×10^{-10} cm^3 s^{-1} at 298 K.[41] The observed rate, which is 2.4 times the kinetic value, indicates a harpooning-type mechanism. Such a mechanism for TM atoms should be viewed with caution as the ionization potentials of TM atoms are relatively large. Valence interactions are expected to play a role to some extent. For example, the rate constant of Ti + SO_2 is smaller than that of Mo + SO_2 even though Ti has a smaller ionization potential than Mo.[13] However, Ti has a $3d^24s^2$ electron configuration which introduces electronic repulsive effects. Reactions involving TM atoms with NO generally proceed with small activation energies. These reactions may proceed through intermediates that preferentially dissociate to products.

An interesting group of reactions is that involving TM atoms + CO_2 and N_2O. With the exception of Nb, all other TM reactions studied thus far are inefficient to varying degrees. The reaction rate constants of Nb + CO_2 and N_2O are at least 200 times larger than those of the other TM + CO_2 and N_2O reactions. Several explanations have been suggested. For example, the inefficient reactions of Ti with CO_2 and N_2O have been attributed to their relatively small electron affinities. A second explanation is that CO_2 and N_2O adiabatically correlate to the excited O(^{1}D) state (and not to the ground state) which may introduce a barrier in these reactions. Another explanation is that some of these reactions do not conserve spin, as in the case of Nb (and Cr and Mo) reacting on the ground state surface with CO_2 (and N_2O):

$$Nb(a^6D_{1/2}) + CO_2(X^1\Sigma_g^+) \rightarrow NbO(X^4\Sigma^-) + CO(X^1\Sigma^+) \quad (7)$$

This explanation deserves attention because Nb and Mo are $4d^{n-1}5s^1$ TM atoms that are adjacent to each other in the periodic table. Mo is unreactive toward CO_2 and N_2O while Nb is very reactive. As one descends from the 3d to the 5d TM series, the validity of the spin quantum number is diminished on account of increased spin−orbit interactions. Russell−Saunders coupling holds reasonably well for Nb.[18] Since Mo is heavier than Nb, it is unlikely that the conservation of spin would be rigorously applied to Mo and not to Nb. (Cr, the lighter group 6 atom, should be seen as obeying Russell−Saunders coupling.) The ground state of NbO follows Hund's case (a), and the low-energy states are quartets and doublets.[63−66] However, visible bands were observed that suggested a tendency toward Hund's case (c) coupling.[63] The spectroscopy of the low-lying electronic states of MoO have been discussed in terms of Hund's case (a) although features were observed in the spectra that suggested a progression toward Hund's case (c).[67] It therefore appears that the conservation of spin should hold in the reaction of Nb with CO_2 and N_2O, but it would not be surprising if the conservation of spin were not obeyed.

A consideration of the electronic structure of TM atoms and the bonding in TMO might provide some insight to the fast Nb + CO_2 and N_2O (and OX) rates. The important bonding TM atomic orbitals in TM oxides are the s and d orbitals. As one moves from left to right across the periodic table, the energy separation of the s and d orbitals increases, a factor that leads to relatively weaker TM−O bonds. There are covalent and ionic components to TM−O bonding. However, covalency generally decreases from left to right in TM series since sd hybridization

is involved.[67−69] For example, in the 3d series the Cu−O bond is mainly ionic whereas TiO has substantial covalency.[69] Nb lies on the left side of the periodic table and thus has a relatively small s−d energy separation. In fact, Nb has the smallest 4d−5s energy separation of all the $4d^{n-1}5s^1$ TM atoms.[67] The closeness of the s and d orbitals enhances hybridization. The ground state is given as $2\delta^2 12\sigma^1\ ^4\Sigma^-$ (4dδ and 5s + 4dσ orbitals).[63,64] This hybridization, coupled with some degree of ionicity, allows Nb to form the strongest bond with atomic oxygen of all the $4d^{n-1}5s^1$ TM atoms.[30] Due to the formation of hybrid orbitals and to the absence of repulsive potentials of a $d^{n-2}s^2$ configuration, as Nb approaches CO_2 (or N_2O) a long-lived complex is expected to be formed. The reaction exothermicity is very high. Thus, many NbO states are energetically accessible; i.e., reaction might take place on multiple surfaces. The intermediate complex lasts long enough such that spin−orbit coupling causes a spin change, and several exit channels are accessed. Additionally, the ground term of Nb has five spin−orbit states, the highest having an energy of only 1050.26 cm^{-1} (see Table 1). In fact, of all the TM atoms with a $d^{n-1}s^1$ orbital occupancy, atomic Nb has the highest density of states in a ground term; energy intervals vary from 154.19 to 355.01 cm^{-1}.[13] Identical rate constants of the *J* states coupled with the small energy differences of the spin−orbit states are highly suggestive of rapid interconversion among the *J* states. Such rapid interconversions may also influence the reactive surface(s). The slower rates of V and Ta, which lie above and below Nb in the periodic table, respectively, with CO_2 (and N_2O) are understood in terms of the $3d^34s^2$ electron configuration. Without knowledge of potential energy surfaces, we are unable to offer plausible explanations for the inefficiencies of the other $d^{n-1}s^1$ TM atoms with CO_2 and N_2O other than their TM−O bond energies are significantly less than that of Nb−O.[30] The lower bond energies imply that covalency and overlap of TM and O atom orbitals are less, and therefore, a sufficiently long-lived complex is not formed.

The growing database of TM + OX rate data indicates that no simple model can describe the reaction mechanisms of TM + OX reactions. We lack a clear explanation for the relative $d^{n-2}s^2$ (and $d^{n-1}s^1$) TM rates as a function of a particular OX and to the relative rates for a particular TM atom as a function of oxidant. At this point, it seems reasonable that the structure and electron affinity of the oxidant, ionization potential of the TM and, perhaps, the promotion energy to a $d^{n-1}s^1$ orbital occupancy, and product states play important roles to varying degrees. An overwhelming, general observation is the enhanced reactivity of $d^{n-1}s^1$ occupancies over those of $d^{n-2}s^2$ occupancies. Since there is some ionic character to TM−O bonding, ionic curves may also play a role. For low IP TM atoms and/or high electron affinity (EA) oxidants, long-range attractions become relatively important, leading to a more attractive surface. For high IP TM atoms and/or low electron affinity oxidants, the crossing of the ionic and covalent curves takes place within the hard-sphere collision diameter and valence effects become more important; i.e., bond strengths, spin−orbit effects, hybridization, etc., determine the outcome of the reactions.

Summary and Conclusions

Our results indicate that Nb is very reactive toward the oxidants O_2, SO_2, CO_2, N_2O, and NO. Ground state rate constants are all on the order of the collision rate. The ground term, Nb($4d^45s^1\ a^6D_J$), depleted faster than the first excited term, Nb($4d^35s^2\ a^4F_J$), in the presence of all the oxidants studied in this work. This was the expected result since the $d^{n-2}s^2$ orbital occupancy is expected to introduce electronic repulsive effects. Niobium ground state was also found to be more reactive than other TM atoms toward the oxidants. This observation is attributed to the orbital occupancy of ground state Nb, the bond strength of the formed niobium monoxide, and a harpooning-type mechanism in the case of SO_2. Nb reacts termolecularly with N_2 and bimolecularly with SF_6. The latter was found to be temperature dependent with an activation energy of 4.8 kcal mol^{-1}.

In general, the $d^{n-1}s^1$ orbital occupancy is a very important factor in the rate of TM + OX reactions. The electronic states of the products as well as the energetics of the reactions are also important, though to varying degrees. Further experimental and theoretical work on TM + OX reactions are needed to corroborate our present understanding of these systems.

Acknowledgment. This research was supported by the Naval Academy Research Council and a Cottrell College Science Award of Research Corporation. Acknowledgment is made to the donors of the Petroleum Research Fund, administered by the American Chemical Society, for partial support of this research. We gratefully acknowledge Skip Gallagher and Thomas E. Bitterwolf of the University of Idaho for providing the $Nb(C_5H_5)(CO)_4$(s). We also express appreciation to Joyce E. Shade of USNA for helping arrange the transfer of the Nb precursor to USNA.

References and Notes

(1) Balasubramanian, K.; Ravimohan, Ch. *J. Phys. Chem.* **1989**, *93*, 4490.
(2) Brown, C. E.; Mitchell, S. A.; Hackett, P. A. *J. Phys. Chem.* **1991**, *95*, 1062.
(3) McClean, R. E.; Pasternack, L. *J. Phys. Chem.* **1992**, *96*, 9828.
(4) McClean, R. E.; Campbell, M. L.; Goodwin, R. H. *J. Phys. Chem.* **1996**, *100*, 7502.
(5) Carroll, J. J.; Weisshaar, J. C. *J. Phys. Chem.* **1996**, *100*, 12355.
(6) Carroll, J. J.; Haug, K. L.; Weisshaar, J. C.; Blomberg, M. R. A.; Siegbahn, P. E. M.; Svensson, M. *J. Phys. Chem.* **1995**, *99*, 13955.
(7) Honma, K.; Nakamura, M.; Clemmer, D. E.; Koyano, I. *J. Phys. Chem.* **1994**, *98*, 13286.
(8) Futerko, P. M.; Fontijn, A. *J. Chem. Phys.* **1991**, *95*, 8065.
(9) Herschbach, D. R. *Adv. Chem. Phys.* **1966**, *10*, 319.
(10) Campbell, M. L. *J. Chem. Phys.* **1996**, *104*, 7515.
(11) Campbell, M. L.; Metzger, J. R. *Chem. Phys. Lett.* **1996**, *253*, 158.
(12) Campbell, M. L.; McClean, R. E. *J. Phys. Chem.* **1993**, *97*, 7942.
(13) Moore, C. E. Atomic Energy Levels as Derived from the Analysis of Optical Spectra. *Natl. Stand. Ref. Data Ser*. (*U.S. Natl. Bur. Stand.*) **1971**, *NSRDS-NBS 35.*
(14) Song, L.; Eychmuller, A.; St. Pierre, R. J.; El-Sayed, M. A. *J. Phys. Chem.* **1989**, *93*, 2485.
(15) Parnis, J. M.; Lafleur, R. D.; Rayner, D. M. *J. Phys. Chem.* **1995**, *99*, 673.
(16) Carroll, J. J.; Haug, K. L.; Weisshaar, J. C. *J. Am. Chem. Soc.* **1993**, *115*, 6962.
(17) Campbell, M. L.; McClean, R. E. *J. Chem. Soc., Faraday Trans.* **1995**, *91*, 3787.
(18) Duquette, D. W.; Hartog, E. A. D.; Lawler, J. E. *J. Quant. Spectrosc. Radiat. Transfer* **1986**, *35*, 281.
(19) $Nb(C_5H_5)(CO)_4$ was obtained from Skip Gallagher and Thomas E. Bitterwolf of the University of Idaho.
(20) Robinson, P. J.; Holbrook, K. A. *Unimolecular Reactions*; Wiley-Interscience: New York, 1972.
(21) Green, D. W.; Korfmacher, W.; Gruen, D. M. *J. Chem. Phys.* **1973,** *58*, 404.
(22) Morse, M. D.; Geusic, M. E.; Heath, J. R.; Smalley, R. E. *J. Chem. Phys.* **1985**, *83*, 2293.
(23) Hamrick, Y.; Taylor, S.; Lemire, G. W.; Fu, Z.-W.; Shui, J.-C.; Morse, M. D. *J. Chem. Phys.* **1988**, *88*, 4095.
(24) Hunt, R. D.; Yustein, J. T.; Andrews, L. *J. Chem. Phys.* **1993**, *98*, 6070.
(25) Bauschlicher, C. W., Jr.; Pettersson, L. G. M.; Siegbahn, P. E. M. *J. Chem. Phys.* **1987**, *87*, 2129.
(26) Moskovits, M.; Ozin, G. A. *J. Chem. Phys.* **1973**, *58*, 1251.
(27) Green, D. W.; Thomas, J.; Gruen, D. M. *J. Chem. Phys.* **1973,** *58*, 5453.
(28) Huber, H.; Kundig, E. P.; Moskovits, M.; Ozin, G. A. *J. Am. Chem. Soc.* **1973**, *95*, 332.

(29) Ozin, G. A.; Voet, A. V. *Can. J. Chem.* **1973**, *51*, 637.
(30) *CRC Handbook of Chemistry and Physics*, 75th ed, Lide, D. R., Ed.; CRC Press: Boca Raton, FL, 1995.
(31) IP(Nb) = 6.77 eV; see ref 13. EA(SF_6) = 1.05 eV; see ref 30.
(32) Herbertson, D. L.; Levy, M. R. *J. Phys. Chem.* **1996**, *100*, 2809.
(33) Talcott, C. O.; Ager, J. W. III; Howard, C. J. *J. Chem. Phys.* **1986**, *84*, 6161.
(34) Husain, D.; Marshall, P. *J. Chem. Soc., Faraday Trans. 2* **1985**, *81*, 613.
(35) Husain, D.; Lee, Y. H. *J. Chem. Soc., Faraday Trans. 2* **1987**, *83*, 2325.
(36) Clay, R. S.; Husain, D. *J. Chem. Res.* **1990**, 384.
(37) Mitchell, S. A.; Hackett, P. A.; Rayner, D. M.; Cantin, M. *J. Phys. Chem.* **1986**, *90*, 6148.
(38) Chowdhury, M. A.; Husain, D. *J. Chem. Soc., Faraday Trans. 2* **1978**, *74*, 1065.
(39) Husain, D.; Sealy, I. P. *J. Photochem.* **1986**, *34*, 245.
(40) Harding, D. R.; Husain, D. *J. Photochem.* **1985**, *28*, 447.
(41) Hard-sphere collision diameters were calculated using data from Hirschfelder et al. (Hirschfelder, J. O.; Curtiss, C. F.; Bird, R. B. *Molecular Theory of Gases and Liquids*; John Wiley & Sons: New York, 1954) and from Fischer (Fischer, C. F. *The Hartree-Fock Method for Atoms*; Wiley: New York, 1977).
(42) Chase, M. W., Jr., Davies, C. A., Downey, J. R., Jr., Frurip, D. J., McDonald, R. A., Syverud, A. N., Eds.; *JANAF Thermochemical Tables*, 3rd ed.; *J. Phys. Chem. Ref. Data*, **1985**, *14* (Suppl. 1).
(43) The list of rate constants is not meant to be exhaustive. We have omitted rate constants that were measured at relatively high temperatures (≈1000 K) such as those measured in shock tubes. Non-Arrhenius behavior is likely over the temperature range 298−1000 K. Therefore, extrapolation from 1000 to 298 K is likely to introduce some error. Reference 8 contains references to other TM + OX reactions at relatively high temperatures.
(44) Ritter, D.; Weisshaar, J. C. *J. Phys. Chem.* **1990**, *94*, 4907.
(45) Clemmer, D. E.; Honma, K.; Koyano, I. *J. Phys. Chem.* **1993,** *97*, 11480.
(46) Narayan, A. S.; Aleksandar, A. G.; Fontijn, A. *Proc. 24th Symp. (Int.) Combust.* **1992**, 727.
(47) Parnis, J. M.; Mitchell, S. A.; Hackett, P. A. *J. Phys. Chem.* **1990**, *94*, 8152.
(48) Fontijn, A.; Blue, A. S.; Narayan, A. S.; Bajaj, P. N. *Combust. Sci. Technol.* **1994**, *101*, 59.
(49) Helmer, M.; Plane, J. M. C. *J. Chem. Soc., Faraday Trans.* **1994**, *90*, 395.
(50) Mitchell, S. A.; Hackett, P. A. *J. Chem. Phys.* **1990**, *93*, 7822.
(51) Narayan, A. S.; Futerko, P. M.; Fontijn, A. *J. Phys. Chem.* **1992**, *96*, 290.
(52) Raiche, G. A.; Belbruno, J. J. *Chem. Phys. Lett.* **1987,** *134*, 341.
(53) Lian, L.; Mitchell, S. A.; Rayner, D. M. *J. Phys. Chem.* **1994**, *98*, 11637.
(54) Campbell, M. L.; McClean, R. E.; Harter, J. S. S. *Chem. Phys. Lett.* **1995**, *235*, 497.
(55) Campbell, M. L. *J. Chem. Soc., Faraday Trans.* **1996**, *92*, 4377.
(56) McClean, R. E.; Campbell, M. L.; Vorce, M. D. Manuscript in preparation.
(57) Campbell, M. L. Manuscript in preparation.
(58) Campbell, M. L.; Hooper, K. L. *J. Chem. Soc., Faraday Trans.*, in press.
(59) Campbell, M. L. Unpublished results.
(60) Harter, J. S. S.; Campbell, M. L.; McClean, R. E. *Int. J. Chem. Kinet.*, in press (unpublished results for W + CO_2).
(61) Campbell, M. L. *J. Phys. Chem.* **1996**, *100*, 19430.
(62) See, for example: Bauschlicher, C. W., Jr.; Langhoff, S. R. *J. Chem. Phys.* **1986**, *85*, 5936.
(63) Brom, J. M., Jr.; Durham, C. H., Jr.; Weltner, W., Jr. *J. Chem. Phys.* **1974**, *61*, 970.
(64) Dyke, J. M.; Ellis, A. M.; Feher, M.; Morris, A.; Paul, A. J.; Stevens, J. C. H. *J. Chem. Soc., Faraday Trans. 2* **1987**, *83*, 1555.
(65) Femenias, J. L.; Cheval, G.; Merer, A. J.; Sassenberg, U. *J. Mol. Spectrosc.* **1987**, *124*, 348.
(66) Cheval, G.; Femenias, J. L.; Merer, A. J.; Sassenberg, U. *J. Mol. Spectrosc.* **1988**, *131*, 113.
(67) Hamrick, Y. M.; Taylor, S.; Morse, M. D. *J. Mol. Spectrosc.* **1991**, *146*, 274.
(68) Merer, A. J. *Annu. Rev. Phys. Chem.* **1989,** *40*, 407.
(69) Bauschlicher, C. W., Jr.; Nelin, C. J.; Bagus, P. S. *J. Chem. Phys.* **1985**, *82*, 3265.